INTERNATIONAL JOURNAL FOR NUMERICAL METHODS IN FLUIDS
Int. J. Numer. Meth. Fluids 2000; **34**: 627–650

Solution of the Navier–Stokes equations in velocity–vorticity form using a Eulerian–Lagrangian boundary element method

D. L. Young*,[1], S. K. Yang and T. I. Eldho

Department of Civil Engineering and Hydrotech Research Institute, National Taiwan University, Taipei, Taiwan, Republic of China

SUMMARY

This paper describes the Eulerian–Lagrangian boundary element model for the solution of incompressible viscous flow problems using velocity–vorticity variables. A Eulerian–Lagrangian boundary element method (ELBEM) is proposed by the combination of the Eulerian–Lagrangian method and the boundary element method (BEM). ELBEM overcomes the limitation of the traditional BEM, which is incapable of dealing with the arbitrary velocity field in advection-dominated flow problems. The present ELBEM model involves the solution of the vorticity transport equation for vorticity whose solenoidal vorticity components are obtained iteratively by solving velocity Poisson equations involving the velocity and vorticity components. The velocity Poisson equations are solved using a boundary integral scheme and the vorticity transport equation is solved using the ELBEM. Here the results of two-dimensional Navier–Stokes problems with low–medium Reynolds numbers in a typical cavity flow are presented and compared with a series solution and other numerical models. The ELBEM model has been found to be feasible and satisfactory. Copyright © 2000 John Wiley & Sons, Ltd.

KEY WORDS: boundary element method; Eulerian–Lagrangian method; Navier–Stokes equations; velocity–vorticity formulation

1. INTRODUCTION

The velocity–vorticity form of the Navier–Stokes equations pioneered by Fasel [1] has been established as an effective formulation for the solution of incompressible viscous flow problems. In the recent times, many researchers used the velocity–vorticity formulation for the calculations of two- and three-dimensional steady and unsteady flows using various numerical methods, such as the finite difference method (FDM) [2], the finite element method (FEM) [3]

* Correspondence to: Department of Civil Engineering, Hydraulic Research Laboratory, National Taiwan University, Taipei 10617, Taiwan, Republic of China.
[1] E-mail: dlyoung@hy.ntu.edu.tw

Received 13 September 1999
Revised 14 February 2000

and the boundary element method (BEM) [4]. In most investigations, the governing equations have been written as a system of parabolic- and Poisson-type equations for the components of the vorticity and velocity fields respectively. The main advantage of this formulation includes the numerical separation of the kinematic and kinetic aspects of the fluid flow from the pressure computation, which is determined afterwards from the known velocity and vorticity fields.

The theoretical potential of the BEM for the solution of Navier–Stokes equations has been adequately exposed by various researchers [5]. In the solution of the velocity–vorticity formulation of the Navier–Stokes equations, two different types of equations (Poisson-type and parabolic-type) are to be solved. While the Poisson-type equations can be accurately solved with the BEM [6], the method is not so stable in the solution of the parabolic-type transport equations [7].

While solving the parabolic-type transport equations, the numerical diffusion and dispersion are the two major problems to be concerned with. The popular methods like the upwind FDM [8] and upwind FEM [9] work well only for the problems in which the diffusion effect dominates. In general, the high-order upwind schemes produce numerical oscillations in the results, while the lower-order upwind schemes cannot avoid the numerical diffusion.

The Eulerian–Lagrangian method is a widely used scheme for the transport modeling. It is a combination of the Eulerian method, in which the equation is solved on a fixed grid in space, and the Lagrangian method, which utilizes either a deforming grid or a fixed grid in deforming co-ordinates. The Eulerian–Lagrangian method (ELM) combines aspects of both approaches so as to merge the simplicity of a fixed Eulerian grid with the computational power of the Lagrangian method [10]. In the transport modeling using the ELM, the advection part is solved by the Lagrangian method, which can be computed independently at each time step by the method of characteristics applied to a grid fixed domain. The remaining diffusion part can be solved by the FEM [10,11] or by the FDM [12], or by the BEM on a separate grid. The influence of the advection is projected from one grid to another by local interpolation.

In the present study, an accurate Eulerian–Lagrangian boundary element method (ELBEM) is proposed for the first time for the velocity–vorticity formulation of the Navier–Stokes equations. The Poisson-type equations are solved using the general boundary integral technique with domain integration for the source terms and from which the vorticity boundary conditions are exactly determined. The vorticity transport equation is solved using the ELBEM on a transformed characteristic domain. Based on the concept of the ELM, the formulation of the ELBEM and its associated fundamental solution is obtained for vorticity transport equations. By combining the ELM and BEM, the BEM is made easier to handle the variable velocity field. In this paper, the interpolation procedure for the ELM computation of the convection part is replaced with the process of the more accurate BEM interior point evaluation, and hence the interpolation error is avoided.

The application of the ELBEM model to incompressible viscous flow problems has been demonstrated using the well-known model problem of flow in a driven square cavity. The cavity flow problem is of continuing interest because it offers a relatively simple model on which numerical techniques may be examined and verified with other numerical schemes. Using the ELBEM model, satisfactory results comparable with other models in literature are presented for Reynolds number of up to 2000.

After presenting the governing equations, the numerical formulation using the ELBEM are briefly described. Then the solution procedure and numerical results for the two-dimensional driven cavity flow problem are described, followed by a few concluding remarks.

2. GOVERNING EQUATIONS

The governing equations for mass and linear momentum transport for an incompressible Newtonian fluid can be written as [13]

$$\frac{\partial \bar{u}}{\partial t} + \bar{u} \cdot \nabla \bar{u} = -\nabla p + \frac{1}{Re} \nabla^2 \bar{u} \tag{1}$$

$$\nabla \cdot \bar{u} = 0 \tag{2}$$

where $\bar{u}$ is the velocity vector, p is the pressure, Re is the Reynolds number and t is the time. Equations (1) and (2) represent the Navier–Stokes equations in the velocity–pressure formulation.

The vorticity vector $\bar{\omega}$ can be expressed as

$$\bar{\omega} = \nabla \times \bar{u} \tag{3}$$

By taking the curl of both sides of Equation (1) and using Equations (2) and (3), we can obtain the vorticity transport equation as follows:

$$\frac{\partial \bar{\omega}}{\partial t} + \bar{u} \cdot \nabla \bar{\omega} = \bar{\omega} \cdot \nabla \bar{u} + \frac{1}{Re} \nabla^2 \bar{\omega} \tag{4}$$

By taking the curl of Equation (3) and using Equation (2) we get

$$\nabla^2 \bar{u} = -\nabla \times \bar{\omega} \tag{5}$$

which is the vector form of Poisson's equation for $\bar{u}$.

Equations (4) and (5), with $\bar{u}$ and $\bar{\omega}$ as velocity and vorticity vectors, are known as the velocity–vorticity formulation of the Navier–Stokes equations, and can replace Equations (1) and (2) in which $\bar{u}$ and p are primitive variables.

We seek a solution in the domain Ω, which satisfies the initial conditions

$$\bar{u} = \bar{u}_0, \qquad \bar{\omega} = \nabla \times \bar{u}_0 \quad \text{at } t = 0 \tag{6}$$

and the boundary conditions

$$\bar{u} = \bar{u}_\Gamma, \qquad \bar{\omega} = (\nabla \times \bar{u})\big|_\Gamma \quad \text{at } t \geq 0 \tag{7}$$

on the boundary Γ of Ω.

For two-dimensional problems, if (u, v) are the velocity vectors $(\bar{u})$ and ω is the associated vorticity, then from Equation (4), the vorticity transport equation can be written as

$$\frac{\partial \omega}{\partial t} + \bar{u} \cdot \nabla \omega = \frac{1}{Re} \nabla^2 \omega \tag{8}$$

Equation (5) can be written as

$$\nabla^2 u = -\frac{\partial \omega}{\partial y} \tag{9}$$

$$\nabla^2 v = \frac{\partial \omega}{\partial x} \tag{10}$$

The solution of the vorticity–transport equation (8), in combination with the velocity Poisson equations (9) and (10) with reference to initial and boundary conditions, gives the velocity and the vorticity distribution all over the domain at the concerned time step.

For the velocity–vorticity formulation, there are certain aspects to be noted [1,14]. Even though the continuity equation has been assumed to be satisfied for the derivation of velocity Poisson equations (9) and (10), it may not be necessarily guaranteed for the integral or difference equations based on the velocity–vorticity formulation. In two-dimensional problems, the continuity equation (2) can be described as

$$D = \frac{\partial u}{\partial x} + \frac{\partial v}{\partial y} = 0 \tag{11}$$

Differentiating Equations (9) and (10) for x and y respectively and adding the resulting equations, we get

$$\frac{\partial^2}{\partial x^2}(D) + \frac{\partial^2}{\partial y^2}(D) = 0 \tag{12}$$

As explained by Fusegi and Farouk [14], from the 'maximum principle' it follows that $|D|$ is maximal on the boundary. It can be concluded that continuity $(D = 0)$ is ensured in the entire integration domain if it is satisfied on the boundary of the problem. Hence, if care is taken to satisfy the continuity condition to a high degree of accuracy on the boundaries, mass conservation is ensured to an even higher accuracy in the interior of the integration domain of the problem. The vorticity definition can be considered in a similar way [1,14]. For the class of problem analyzed in the present investigations, and by the assumption of no-slip walls on the boundaries, the continuity condition is automatically satisfied.

3. NUMERICAL FORMULATION

As mentioned earlier, in the solution of the velocity–vorticity formulation of Navier–Stokes equations using the present model, the vorticity transport equation (8) is solved using the ELBEM and the Poisson-type velocity equations (9) and (10) are solved using the boundary integral equation scheme. In this section, the numerical formulation is briefly described.

3.1. BEM formulation of velocity Poisson equations

Consider the Poisson-type velocity equation in u and ω, say Equation (9)

$$\nabla^2 u = -\frac{\partial \omega}{\partial y} = b \tag{13}$$

with velocity boundary conditions as

$$u = u_0 \quad \text{on } \Gamma_1, \qquad q_0 = \frac{\partial u_0}{\partial n} \quad \text{on } \Gamma_2 \tag{14}$$

where n is the unit outward normal vector. In the present model, an iterative scheme is used such that the vorticity is known in the current iteration and time step from the previous step by solving the vorticity transport equation (8).

Considering $u^* = \ln(r)$ as the fundamental solution of the Laplace equation in two dimensions, from Green's theorem, the boundary integral equation for Equation (13) can be written as

$$C_i u_i = \int_\Gamma u q^* \, \mathrm{d}\Gamma - \int_\Gamma q u^* \, \mathrm{d}\Gamma + \int_\Omega b u^* \, \mathrm{d}\Omega \tag{15}$$

where C_i is Green's constant, $q = \partial u/\partial n$, $q^* = \partial u^*/\partial n$ and r is the distance from the collocation point (k) to other field points (i), defined as

$$r = \sqrt{(x_k - x_i)^2 + (y_k - y_i)^2} \tag{16}$$

Considering Equation (13), $b = -(\partial \omega/\partial y)$. In Equation (15), let the domain integral be represented as

$$B = \int_\Omega -\frac{\partial \omega}{\partial y} u^* \, \mathrm{d}\Omega \tag{17}$$

Now from Green's theorem, we can write Equation (17) as

$$B = +\int_\Omega \omega \frac{\partial u^*}{\partial y} \, \mathrm{d}\Omega + \int_\Gamma \omega u^* \, \mathrm{d}x \tag{18}$$

Now $\partial u^*/\partial y$ can be found as

$$\frac{\partial \ln(r)}{\partial y} = \frac{y_k - y_i}{(x_k - x_i)^2 + (y_k - y_i)^2} \tag{19}$$

Therefore, Equation (18) can be written as

$$B = + \int_\Omega \omega \frac{y_k - y_i}{(x_k - x_i)^2 + (y_k - y_i)^2} \, \mathrm{d}\Omega + \int_\Gamma \omega u^* \, \mathrm{d}x \tag{20}$$

Now we can write Equation (15) as

$$C_i u_i = \int_\Gamma u q^* \, \mathrm{d}\Gamma - \int_\Gamma q u^* \, \mathrm{d}\Gamma + \int_\Omega \omega \frac{y_k - y_i}{(x_k - x_i)^2 + (y_k - y_i)^2} \, \mathrm{d}\Omega + \int_\Gamma \omega u^* \, \mathrm{d}x \tag{21}$$

In a similar way, the boundary integral equation for Equation (10) can be derived using Green's theorem as

$$C_i v_i = \int_\Gamma v q^* \, \mathrm{d}\Gamma - \int_\Gamma q' u^* \, \mathrm{d}\Gamma - \int_\Omega \omega \frac{x_k - x_i}{(x_k - x_i)^2 + (y_k - y_i)^2} \, \mathrm{d}\Omega + \int_\Gamma \omega u^* \, \mathrm{d}y \tag{22}$$

where $q' = \partial v/\partial n$.

In Equations (21) and (22), we have boundary integrals and domain integrals. In the present model, the domain integration is carried out by sub-dividing the domain into a series of internal cells, on each of which a numerical integration is performed. Here linear elements are used for the boundary discretization and two-dimensional isoparametric quadrilateral cells are used for the internal discretization. The details of the element properties, shape functions, co-ordinate transformation and numerical integration used here are described in Brebbia *et al.* [6], which are not repeated here.

Here, considering Equation (21), if the domain is discretized into L internal cells, then the domain integral can be written as

$$D_i = \int_\Omega \omega \frac{y_k - y_i}{(x_k - x_i)^2 + (y_k - y_i)^2} \, \mathrm{d}\Omega = \sum_{e=1}^{L} \left[\sum_{k=1}^{\mathrm{NI}} w_k \left(\omega \frac{y_k - y_i}{(x_k - x_i)^2 + (y_k - y_i)^2} \right)_k \right] \Omega_e \tag{23}$$

where the integral has been approximated by a summation over different cells (e varies from 1 to L), w_k are the Gauss integration weights, the function needs to be evaluated at integration points k on each cell (k varies from 1 to NI, where NI is the total number of integration points on each cell) and Ω_e is the area of cell e. The term D_i is the result of the numerical integration and is different for each position i of the boundary nodes.

Assuming that the boundary of the domain is discretized into NE linear elements with N nodes, Equation (21) can be discretized and written in matrix form as

$$-C_i u_i + \sum_{j=1}^{N} \bar{H}_{ij} u_j + D_i = \sum_{j=1}^{N} (G_{ij} q_j - P_{ij} \omega_j) \tag{24}$$

Combining the effect of the constant term C with the $\bar{H}$ matrix, we can write the system of matrix as

$$Hu + D = Gq - P\omega \tag{25}$$

In Equation (25), the boundary conditions are introduced and the known values are taken to the right-hand side to form a system of linear equations of the form

$$AX = F \tag{26}$$

where X is a vector of unknown boundary values of u and q, and F is a known vector. Equation (26) is solved using a Gauss elimination scheme and all the boundary values will be then known. Once this is done, it is possible to calculate internal values of u or its derivatives. The values of u are calculated at any internal point using Equation (24). Similar procedures are used to calculate the values of v at any internal point using Equation (22).

The main advantage of using the BEM in the solution of the velocity Poisson equations is the exact determination of the vorticity boundary conditions from the velocity flux values that are obtained by the solution of Equation (25). The vorticity boundary condition that is essential to solve the vorticity transport equation is directly obtained as the velocity normal derivative from the solution of Equations (21) and (22), together with the no-slip boundary conditions. If other numerical methods like the FDM or the FEM are used in the solution of velocity Poisson equations, then the vorticity values are to be separately calculated from the velocity values. By doing so, computational error for vorticity may be introduced. Besides, the accuracy of the vorticity boundary conditions is very crucial for the convergence of the velocity–vorticity formulation.

3.2. ELBEM formulation of vorticity transport equation

The vorticity transport equation (8) is very similar to the form of unsteady convective diffusion equation for transport phenomena [Young DL, Wang YF, Eldho TI. Solution of the advection diffusion equation using the Eulerian–Lagrangian boundary element method. *Engineering Analysis with Boundary Elements* 2000 (in press)]. For the solution of Equation (8), the initial and boundary conditions should be prescribed. The initial condition, usually prescribed vorticity, is described throughout the domain at some initial time as

$$\omega = \omega_i(\bar{x}) \quad \text{in } \Omega, \quad t = 0 \tag{27}$$

Two common types of boundary conditions prescribed are

$$\omega = \omega_0(t) \quad \text{on } \Gamma_t, \quad 0 < t \tag{28}$$

$$q = -\frac{1}{Re}\frac{\partial \omega}{\partial n} + (\bar{u}\omega)\cdot\bar{n} = q_0(t) \quad \text{on } \Gamma_q, \quad 0 < t \tag{29}$$

where q is the normal flux, Ω is the domain and $\Gamma = (\Gamma_t \cup \Gamma_q)$ the boundary.

Owing to the Eulerian–Lagrangian concept, the computational domain is now chosen along the characteristic domain, as shown in Figure 1. The vorticity transport equation is rewritten by a hydrodynamic derivative within this new domain as

$$\frac{\mathrm{D}\omega}{\mathrm{D}t} = \frac{1}{Re}\nabla^2\omega \quad \text{in } \Omega_E \tag{30}$$

where the hydrodynamic derivative is defined as

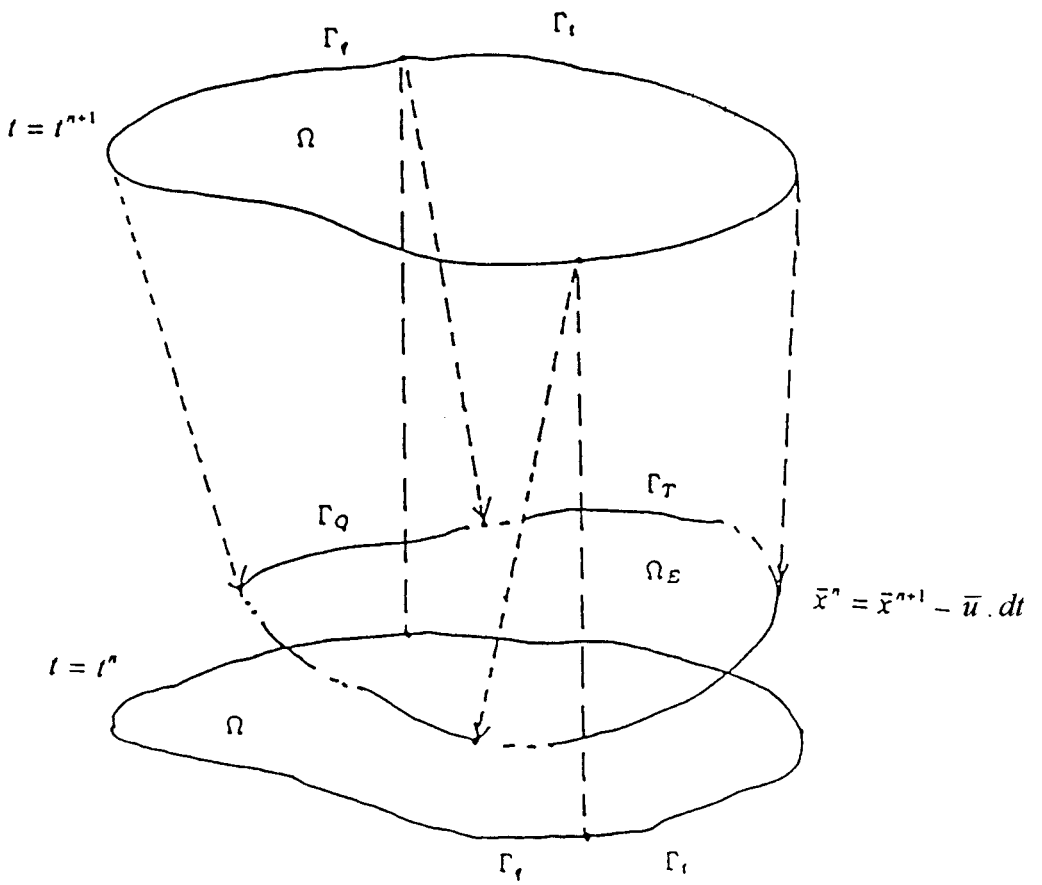

Figure 1. Characteristic domain and boundaries.

$$\frac{\mathrm{D}}{\mathrm{D}t} = \frac{\partial}{\partial t} + \bar{u} \cdot \nabla \tag{31}$$

The initial and boundary conditions are now defined as

$$\omega = \omega_i(\bar{x}) \quad \text{in } \Omega_E, \quad t = 0 \tag{32}$$

$$\omega = \omega_0(t) \quad \text{on } \Gamma_T, \quad 0 < t \tag{33}$$

$$q = -\frac{1}{Re}\frac{\partial \omega}{\partial n} = q_0(t) \quad \text{on } \Gamma_Q, \quad 0 < t \tag{34}$$

Now using Green's second identity, the boundary integral equation can be derived on the characteristic domain as

$$\alpha(\bar{x}_i, t^{n+1})\omega(\bar{x}_i, t^{n+1}) = \int_{t^n}^{t^{n+1}} \int_{\Gamma} \hat{q}(\bar{x}_i, t^n;\ \bar{x}, t)\omega(\bar{x}, t)\, \mathrm{d}\Gamma_E\, \mathrm{d}t$$
$$- \int_{t^n}^{t^{n+1}} \int_{\Gamma} \hat{\omega}(\bar{x}_i, t^n;\ \bar{x}, t)q(\bar{x}, t)\, \mathrm{d}\Gamma_E\, \mathrm{d}t + \int_{\Omega E} \hat{\omega}(\bar{x}_i, t^{n+1};\ \bar{x}, t^n)\omega(\bar{x}, t^n)\, \mathrm{d}\Omega_E \tag{35}$$

in which α is the Cauchy principle value, $\bar{x}_i$ is the position vector of base point, $\bar{x}$ is any field point, and q and $\hat{q}$ are the flux terms defined in the following equations:

$$q(\bar{x}, t) = -\frac{1}{Re}\frac{\partial \omega}{\partial n} \tag{36}$$

$$\hat{q}(\bar{x}, t) = -\frac{1}{Re}\frac{\partial \hat{\omega}}{\partial n} \tag{37}$$

The associated fundamental solution $\hat{\omega}$ satisfies the source varying formally adjoint operator of the governing equation (30). That is

$$\frac{\mathrm{D}\hat{\omega}}{\mathrm{D}t} - \frac{1}{Re}\nabla^2\hat{\omega} = \delta(\bar{x} - \bar{x}_i)\delta(t - t^n) \tag{38}$$

Now the fundamental solutions can be easily derived for the one-, two- and three-dimensional problems [15]

$$\hat{\omega}(\bar{x}, t;\ \bar{x}_i, t^n) = \frac{Re}{[4\pi(t - t^n)]^{k/2}} \exp\left[-\frac{Rer^2}{4(t - t^n)}\right] \tag{39}$$

where $r = |\bar{x} - \bar{x}_i|$ is the Cartesian distance between the base point and the any field point. For one-, two- and three-dimensional problems, k is equal to 1, 2 and 3 respectively.

The integral equation (35) implies that the boundary conditions and initial condition are treated as a continuous distribution of the impulse acting on the domain boundary. The third term on the right-hand side of the integral equation (35), which is in the form of a volume integral, represents the initial effect of the transport equation. The first and second terms on the right-hand side, which are in the form of boundary integrals, express the induced effect of the Dirichlet and Neumann boundary conditions.

For each time step t^{n+1}, the computational domain Ω_E coincides with the physical domain Ω only at $t = t^{n+1}$, and the boundary conditions and initial condition are given on the physical boundary Γ, and the physical domain Ω of time step $t = t^n$. However, the boundary and initial values are required to be imposed in integral terms of Equation (35) on the computational characteristics boundary Γ_E ($\Gamma_T \cup \Gamma_Q$), and the domain Ω_E of time step $t = t^n$. The region of the characteristic domain is determined by the method of characteristics as

$$\frac{\mathrm{d}\bar{x}}{\mathrm{d}t} = \bar{u} \tag{40}$$

$$\bar{x}^n = \bar{x}^{n+1} - \bar{u} \cdot \mathrm{d}t \tag{41}$$

The higher-order fractional step technique, or the Runge–Kutta scheme if necessary, could be used to improve the accuracy of the integration with respect to the time domain.

The boundary element approach [6] is used to solve the boundary integral equation (35) and its associated boundary and initial conditions. Constant, or linear or quadratic shape functions can be used to discretize [6] the temporal and spatial domain respectively, as

$$\omega(\bar{x}, t) = F(t)\omega(\bar{x}, t^{n+1}), \quad F(t) = 1 \quad \text{at } t^n \le t \le t^{n+1} \quad \text{on } \Gamma_T \quad \text{and} \quad \Gamma_Q \tag{42}$$

$$q(\bar{x}, t) = F(t)q(\bar{x}, t^{n+1}), \quad F(t) = 1 \quad \text{at } t^n \le t \le t_k \quad \text{on } \Gamma_T \quad \text{and} \quad \Gamma_Q \tag{43}$$

$$\omega(\bar{x}, t^{n+1}) = \sum_{j=1}^{N} S_j(\bar{x})\omega(\bar{x}_j, t^{n+1}) \quad \text{at } t = t^{n+1} \quad \text{on } \Gamma_T \quad \text{and} \quad \Gamma_Q \tag{44}$$

$$q(\bar{x}, t^{n+1}) = \sum_{j=1}^{N} S_j(\bar{x})q(\bar{x}_j, t^{n+1}) \quad \text{at } t = t^{n+1} \quad \text{on } \Gamma_T \quad \text{and} \quad \Gamma_Q \tag{45}$$

$$\omega(\bar{x}, t) = \sum_{i=1}^{M} T_i(\bar{x})\omega(\bar{x}_i, t) \quad \text{at } t^n \le t \le t^{n+1} \quad \text{on} \quad \Gamma_T \quad \text{and} \quad \Gamma_Q \tag{46}$$

where N is the number of the boundary nodes and M is the number of nodes of the discretization of the volume integral and S and T are all the corresponding shape functions for space. The use of constant elements for the temporal domain allows the analytic integral of time [6] in Equation (35).

After approaching the base point included in the integral equation (35) to the boundary nodes on Ω_E at $t = t^{n+1}$, and imposing the boundary conditions and initial conditions, a simultaneous equations system can be written in the matrix form as

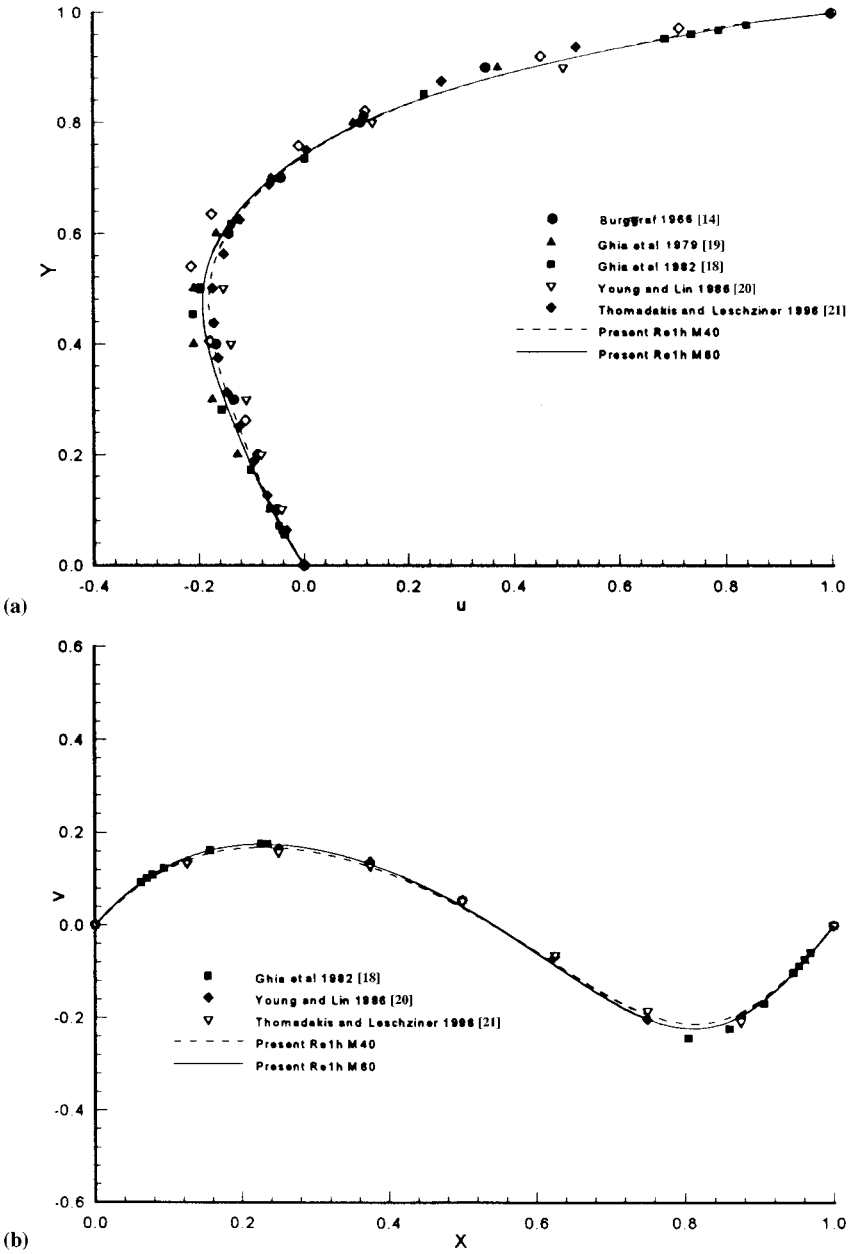

Figure 2. Profile of u (a) and v (b) along the cavity vertical and horizontal centerline of a square cavity for $Re = 100$.

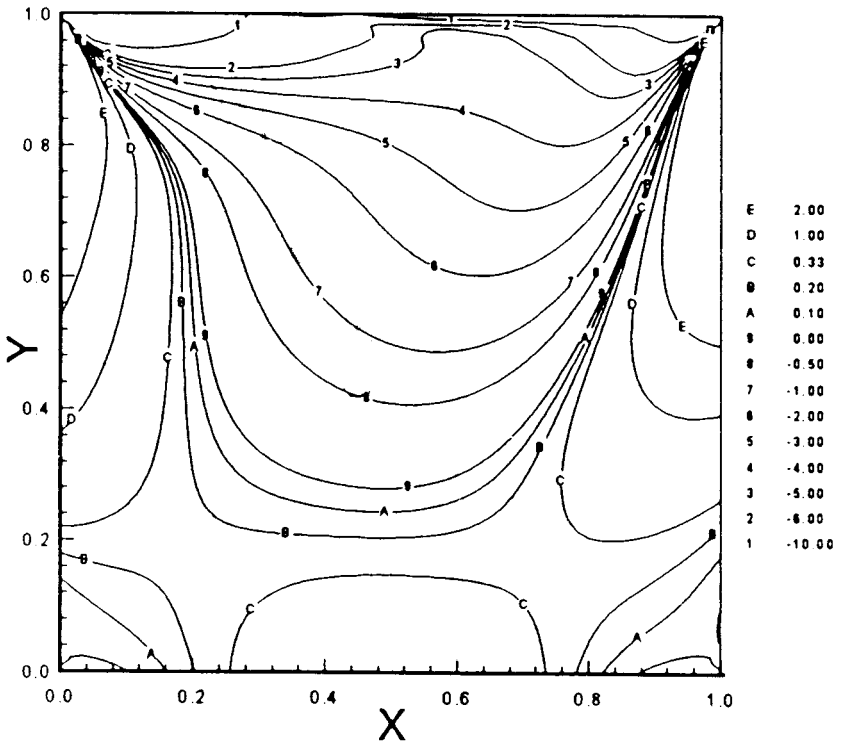

Figure 3. Vorticity distribution for $Re = 100$.

$$[A]_{N\times L1}\{\omega\}_{L1\times 1} + [B]_{N\times L2}\{q\}_{L2\times 1} = \{\mathrm{RHS}\}_{N\times 1} \tag{47}$$

in which L_1 and L_2 are the unknown values of ω and q respectively, and $L_1 + L_2 = N$. If the time difference is the same, the elements included in the matrices $[A]$ and $[B]$ will not be changed for every time step. Only the right-hand side vector $\{\mathrm{RHS}\}$ should be evaluated for each time step due to the changes of the time-dependent boundary conditions and the solutions of the previous time step solutions.

3.3. Determination of streamfunction

The streamfunction distribution of the two-dimensional fluid flow is determined from the following formula:

$$\nabla^2\psi = -\omega \tag{48}$$

where ψ is the streamfunction. Similar to the BEM formulation of velocity Poisson equations in Section 3.1, the boundary integral equation for Equation (48) can be written as

$$C_i\psi_i = \int_\Gamma \psi \frac{\partial \ln(r)}{\partial n}\, d\Gamma - \int_\Gamma \frac{\partial \psi}{\partial n} \ln(r)\, d\Gamma - \int_\Omega \omega \ln(r)\, d\Omega \tag{49}$$

After the vorticity distribution is determined by solving the vorticity transport equation by introducing the appropriate boundary conditions, the streamfunction distribution can be determined by solving the boundary integral equation (49).

4. SOLUTION PROCEDURE

As mentioned earlier, here an iterative scheme is used in the solution of the velocity–vorticity formulation of Navier–Stokes equations. In most of the incompressible viscous flow problems solved using Navier–Stokes equations, the most natural boundary condition arises when the velocity is prescribed all over the boundaries of the problem. The vorticity boundary conditions are seldom prescribed and hence should be determined iteratively from computations. In the present model, the velocity Poisson equations are initially solved to get the vorticity boundary conditions, which are used in the solution of the vorticity transport equation. The computational procedure adopted here includes the following iterative steps:

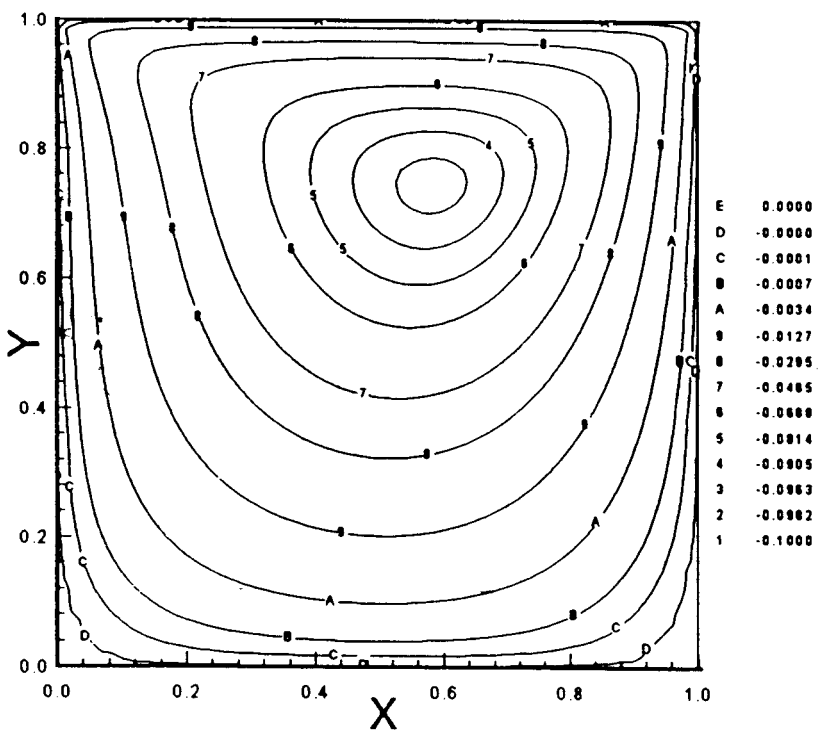

Figure 4. Streamfunction distribution for $Re = 100$.

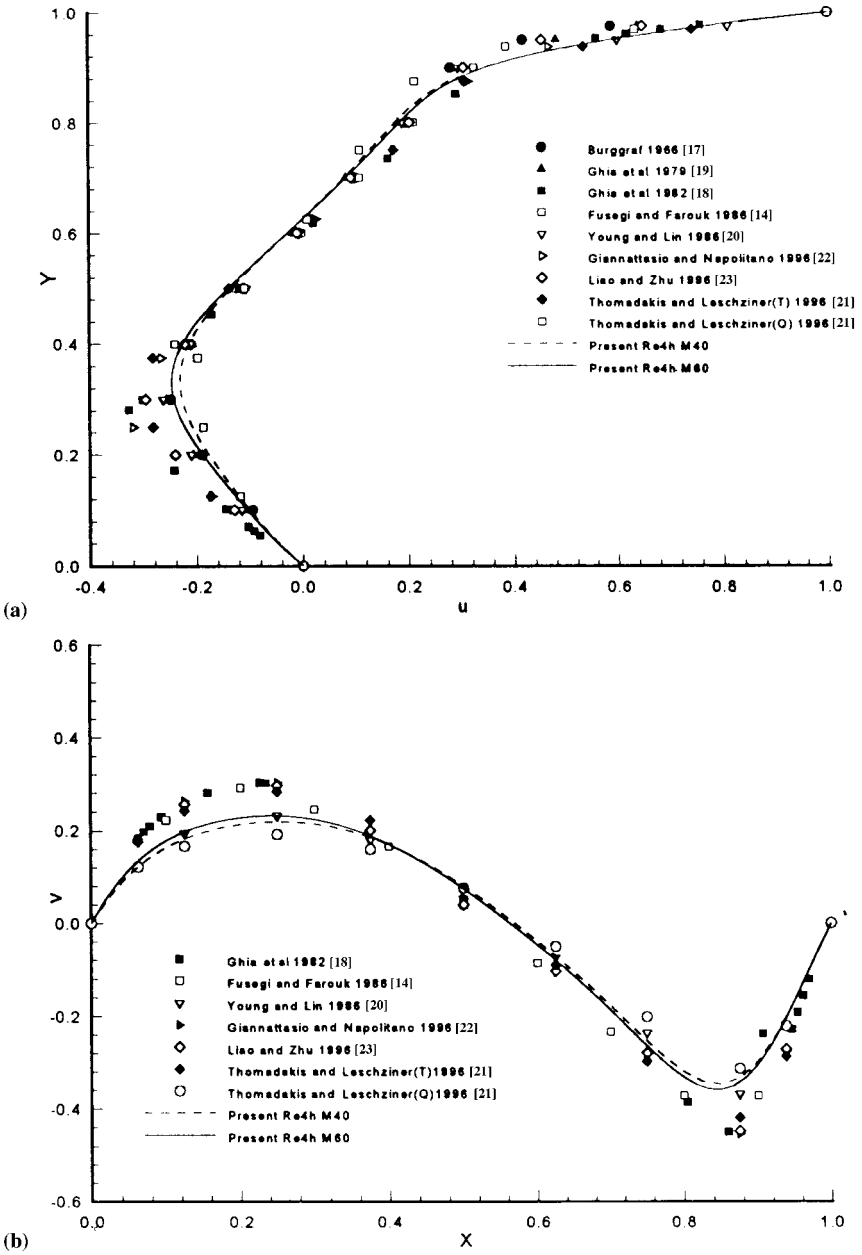

Figure 5. Profile of u (a) and v (b) along the cavity vertical and horizontal centerline of a square cavity for $Re = 400$.

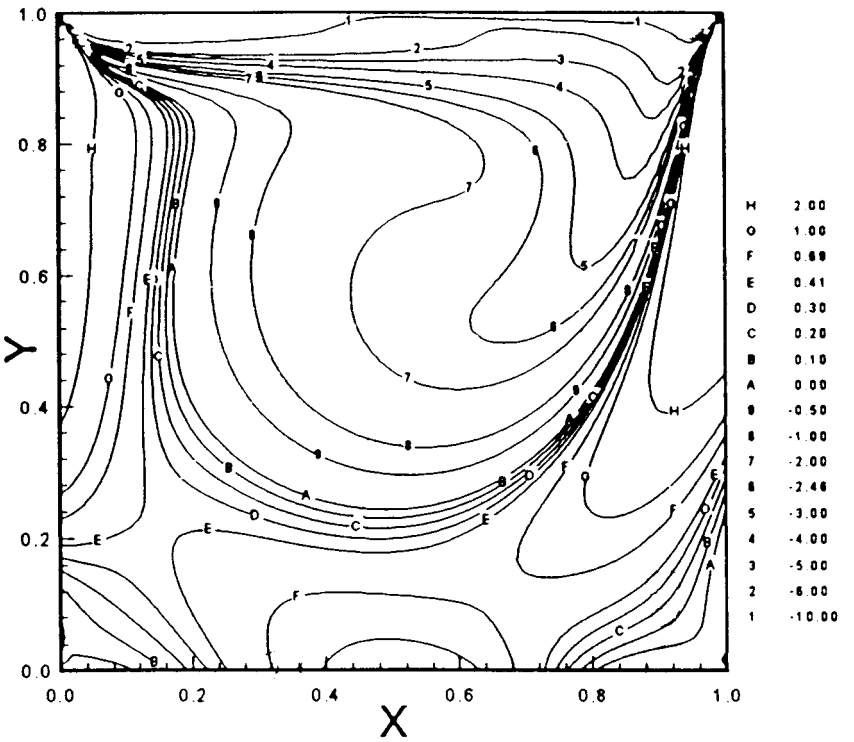

Figure 6. Vorticity distribution for $Re = 400$.

For the time step $n = 1$

1. Assume some initial values for vorticity distribution and derivatives, say zero.
2. Solution of the velocity Poisson equations using the BEM
   - Solve for the unknown boundary velocity or velocity flux values using Equations (9) and (10)
   - Calculate the velocity distribution and velocity derivatives at all nodal points
   - Determine the new vorticity boundary values using Equation (3)
3. Solution of the vorticity transport equations using the ELBEM
   - Solve for the unknown vorticity values throughout the domain using Equation (8)
   - Relax the vorticity values, if necessary
4. Check for convergence of the velocity and vorticity components in the present iteration, for example

$$\frac{|u_n^{k+1} - u_n^k|}{|u_n^k|} \leq 0.001$$

If convergence criterion is satisfied, then stop and proceed to the next time step, otherwise go to step 2.

5. In the successive time step, use the velocity and vorticity components from the previous time step as initial conditions and use the iterative procedure, steps 2–4. The procedure is repeated until the prescribed time step is reached.

In order to validate the self-consistency of the present formulation, calculations were made to ensure the satisfaction of mass balance conditions in the entire domain for all the computations. In all the calculations, mass balances were satisfied within 0.1 per cent.

For the unsteady computations, the time step was chosen with variations in Reynolds number and the mesh size, according to the condition given by Liu and Dane [16] as

$$\frac{1}{Re}\,\Delta t\left(\frac{1}{(\Delta x)^2}+\frac{1}{(\Delta y)^2}\right)\leq\frac{1}{2} \tag{50}$$

where Δx and Δy are the mesh size in the x- and y-Cartesian directions.

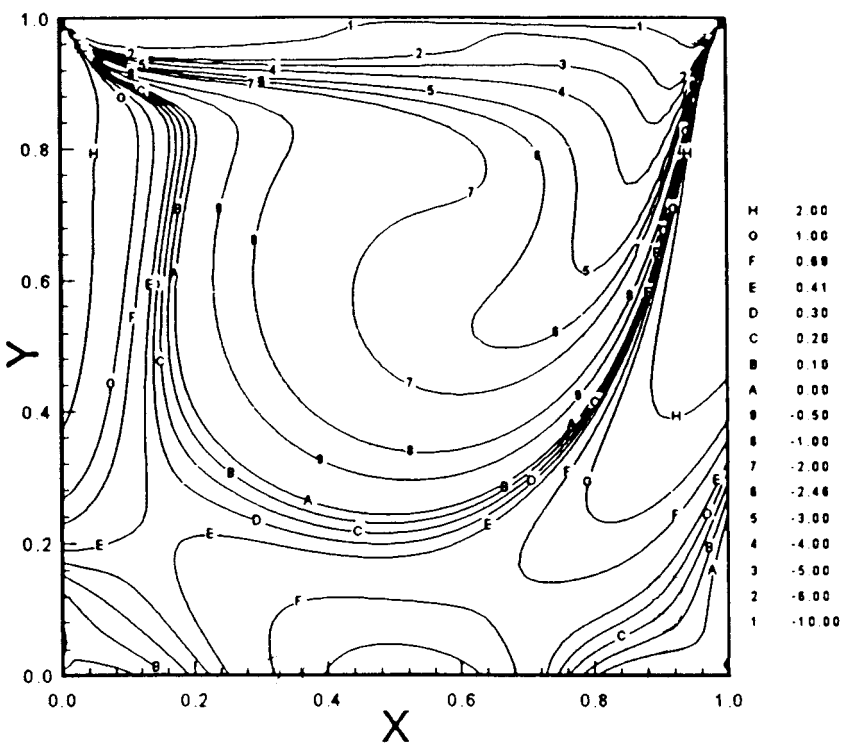

Figure 7. Streamfunction distribution for $Re = 400$.

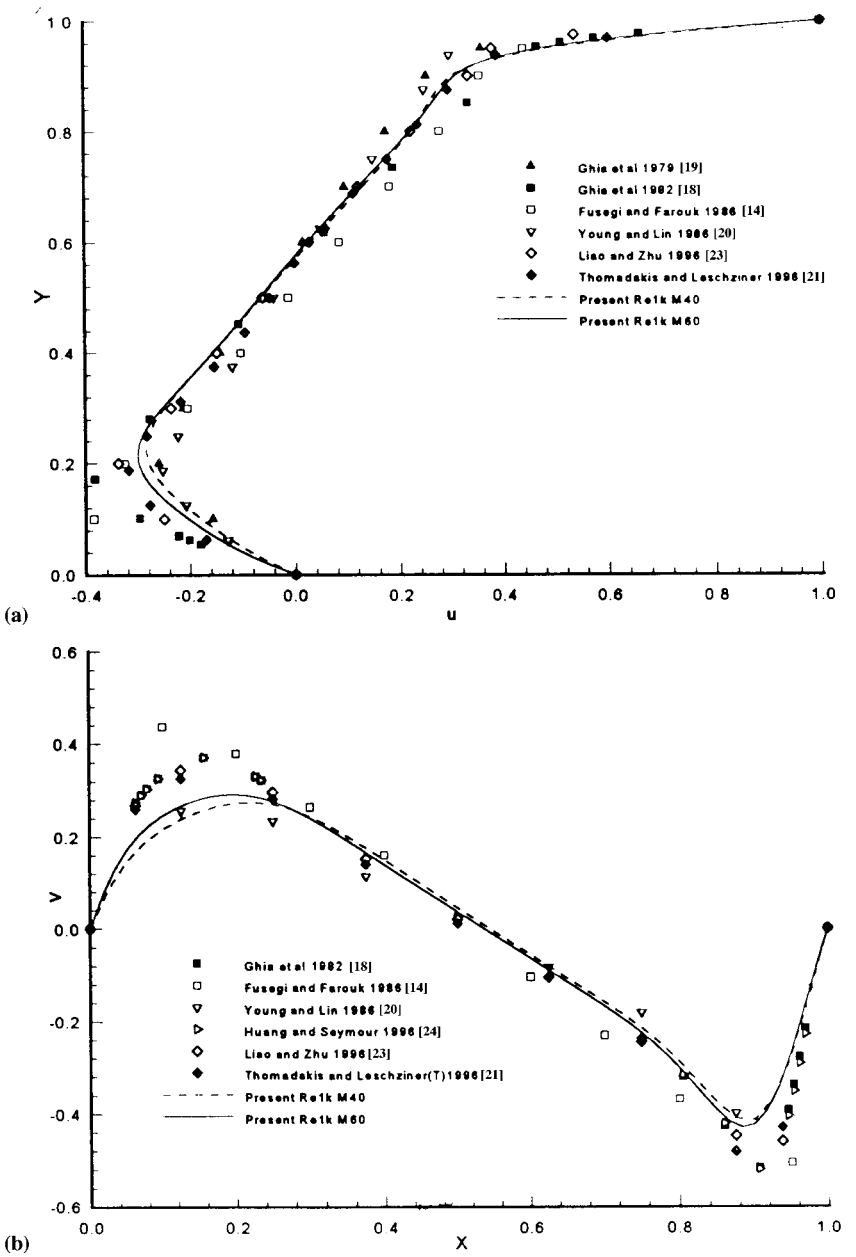

Figure 8. Profile of u (a) and v (b) along the cavity vertical and horizontal centerline of a square cavity for $Re = 1000$.

5. MODEL RESULTS AND DISCUSSIONS

The proposed ELBEM model has been applied on a test problem to verify the feasibility of the model. The test problem is the classical 'driven flow in a square cavity', for which many numerical model results are available in the literature. Present model results are compared with the results of a series solution and FDM, FEM and BEM models in two dimensions.

The model problem consists of a square cavity with a moving top lid with constant velocity, totally filled with an incompressible viscous fluid. In all the cases, the flow inside the cavity was initially at rest. No-slip and impermeability conditions were imposed on all walls, with the velocity at the upper wall set equal to unity. Due to the computational limitations (we used an IBM AIX workstation with 128 MB RAM), the present analysis is limited to a maximum computational mesh points of 60×60 (on the boundary as well as internal domain).

Four analyses have been presented here, for $Re = 100$, 400, 1000 and 2000 respectively. Although the computations were carried out in time, only steady state solutions are presented here. In all the cases, steady states are reached.

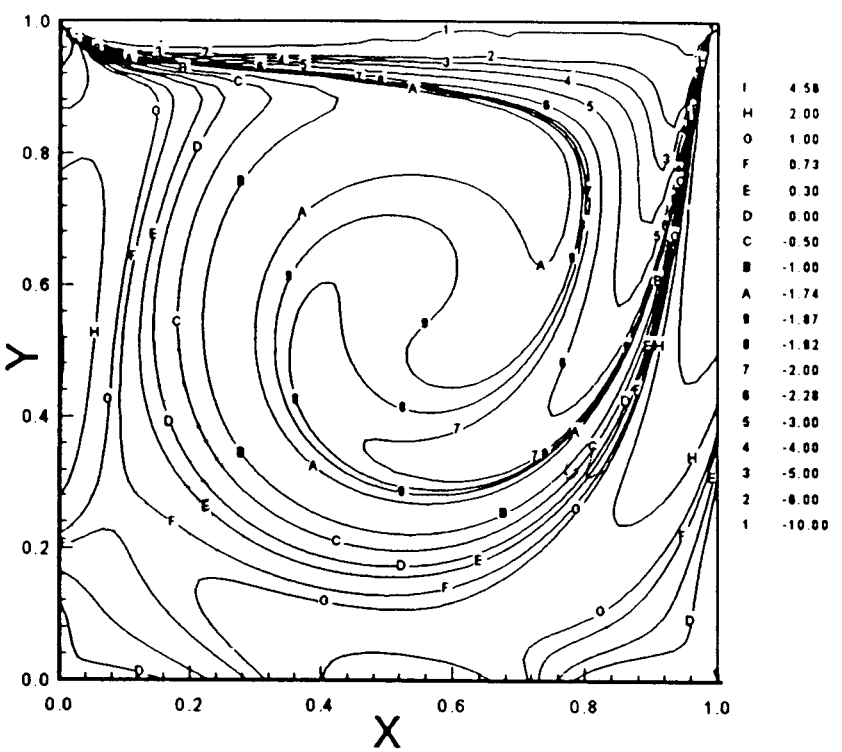

Figure 9. Vorticity distribution for $Re = 1000$.

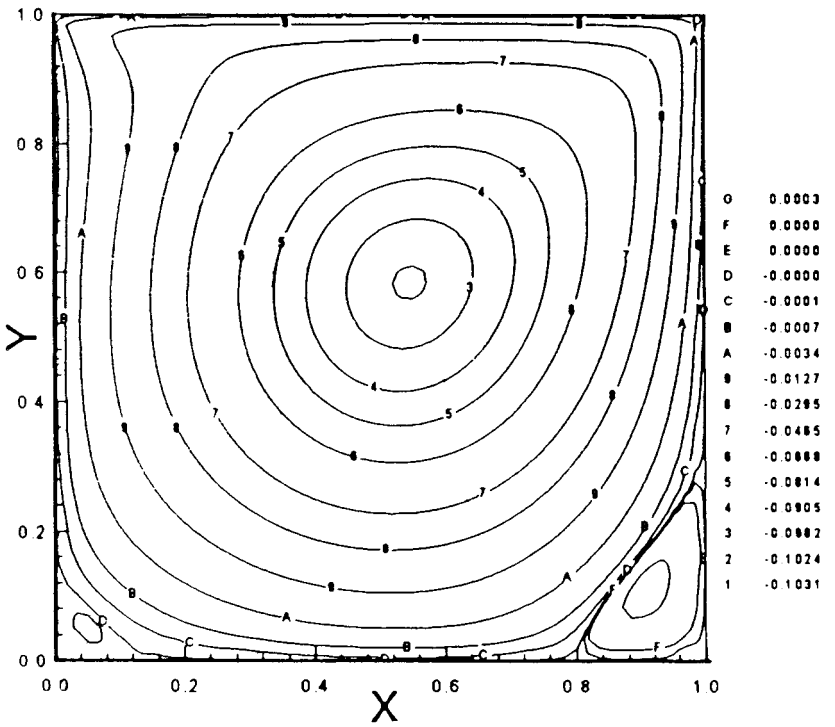

Figure 10. Streamfunction distribution for $Re = 1000$.

Figure 2 shows the u- and v-velocity profiles along the vertical and centerlines of the cavity for $Re = 100$. Two different grids of 40×40 and 60×60 uniform quadrilaterals have been used for the computations. Figure 3 shows the vorticity distribution along the domain and Figure 4 shows the profile of the streamfunction distribution along the domain. The velocity variations are compared with different models of Burgraff [17], Ghia *et al.* [18,19], Young and Lin [20] and Thomadakis and Leschziner [21]. The results mostly agree with all the model results. From Figure 2 it can be seen that for both computational mesh grids, the results are almost the same.

Figure 5 shows the u- and v-velocity profiles along the vertical and centerlines of the cavity for $Re = 400$ with two different grids of 40×40 and 60×60 uniform quadrilaterals. Figures 6 and 7 show the vorticity and streamfunction distributions respectively along the domain. The velocity variations are compared with different models of Burgraff [17], Ghia *et al.* [18,19], Fusege and Farouk [14], Young and Lin [20], Giannattasio and Napolitano [22], Liao and Zhu [23], and Thomadakis and Leschziner [21]. The results obtained are closer to the results of the FEM and the finite volume models. As is obvious from the figures, the small difference to other models can be attributed to the mesh size used in the present investigation.

As the Reynolds number increases, the sensitivity to the grid density becomes more obvious. For a higher Reynolds number, $Re = 1000$, Figure 8 shows the x-component velocity profile (u) and y-component velocity profile (v) on the vertical and horizontal centerline of the cavity. Figures 9 and 10 show the vorticity and streamfunction distributions respectively along the domain. Results of the analysis are again compared with the various models [14,18–21,23,24]. The present analysis is in good agreement with most of the models, bearing in mind that the maximum mesh density was only 60×60. Further analysis has been carried out for a Reynolds number of 2000 using 60×60 mesh. Figures 11–13 show the vorticity, streamfunction and velocity distributions respectively along the domain.

The merit of the present model is that it provides the best way to treat the velocity–vorticity formulation for two-dimensional flow by the BEM. In general, the boundary conditions of vorticity are not known *a priori*, so that the solution of the vorticity transport equation is rather difficult. However, the BEM solution of the velocity Poisson equations together with the no-slip boundary conditions will automatically render the necessary vorticity boundary conditions directly as the normal derivatives of velocity, while solving the boundary integral equations. If numerical models like FDM and FEM are used in the solution of velocity

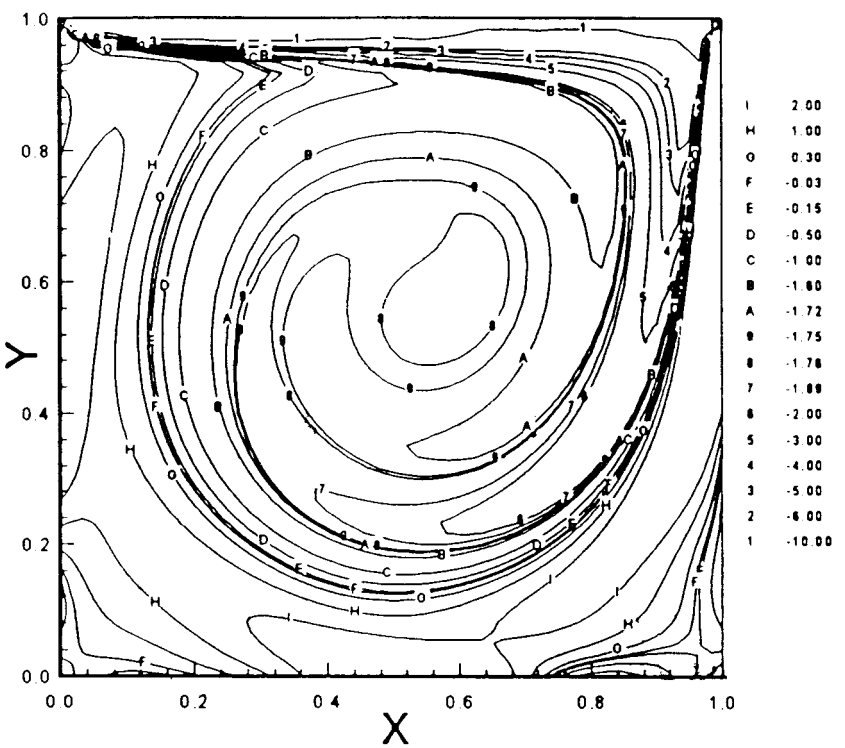

Figure 11. Vorticity distribution for $Re = 2000$.

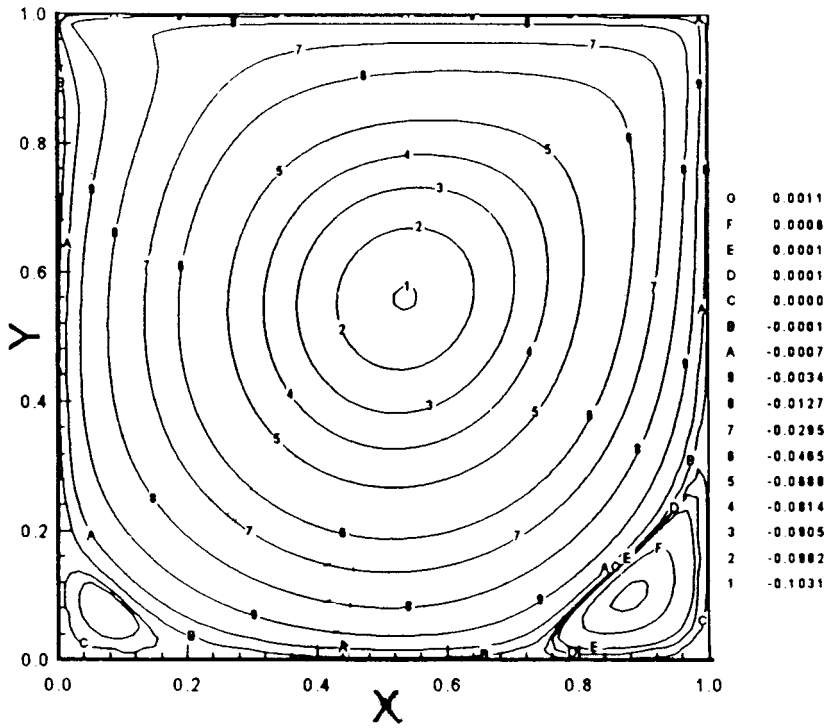

Figure 12. Streamfunction distribution for $Re = 2000$.

Poisson equations, then the boundary vorticity values have to be separately determined from the velocity distribution, which may reduce the accuracy in determining the vorticity boundary conditions for the solution of vorticity transport equation.

As the vorticity transport equation includes convective terms and time-dependent terms, the general BEM solution [5,6] of vorticity transport equation is very difficult. The ELBEM, proposed by combining the Eulerian–Lagrangian method and the BEM, has been proved to be a feasible method to solve advective–diffusion equations such as the vorticity transport equation [Young *et al.*]. Hence, the present model in which the velocity Poisson equations are solved using the BEM and the vorticity transport equation is solved using ELBEM and the iterative scheme combining both models provides the best way to treat the velocity–vorticity formulation for two-dimensional incompressible flow problems. This study demonstrates that even with a relatively coarse mesh, the solutions are very stable and fairly accurate as shown in the case study with different Reynolds numbers.

The approximate number of iterations required for the convergence at each time step vary from 50 to 500 depending on the value of the Reynolds number, time step and grid. Even though the CPU time for each calculation has not been separately found out, typical CPU time for the calculation varies from 1 to 6 h on an IBM AIX workstation for 60×60 mesh.

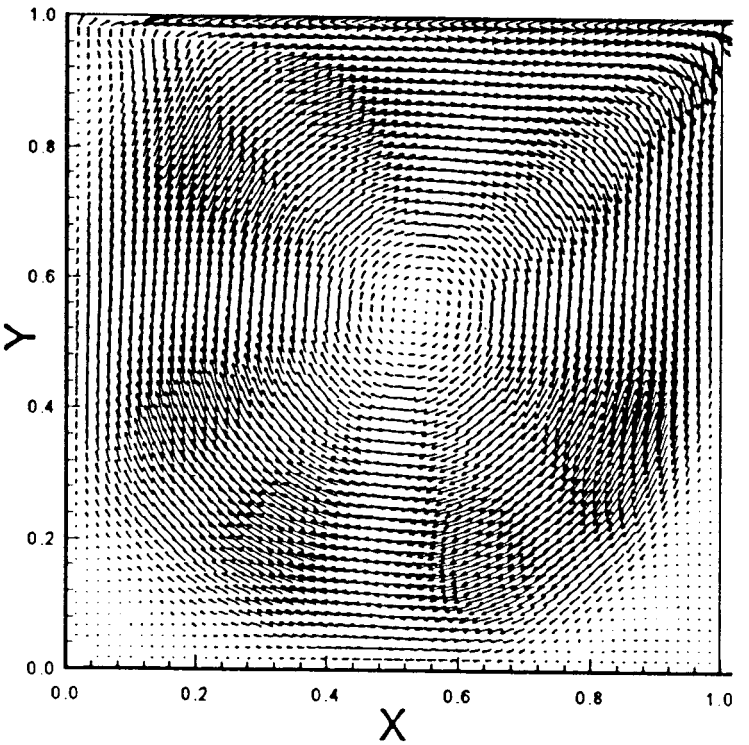

Figure 13. Profile of the flow vectors for $Re = 2000$.

Even though in the present analysis we have carried out the analysis up to a Reynolds number of 2000, the method can be further used for higher Reynolds number with a refined mesh, smaller time step and vorticity relaxation. The ELBEM has already been successfully implemented for three-dimensional diffusion and advection problems [25; Young DL, Her BC, Eldho TI. Boundary integral modeling of three-dimensional circulation and transport in stratified estuaries. *Journal of Engineering Mechanics*, *ASCE* 2000 (in press)]. Authors also have successfully implemented the velocity–vorticity formulation for the Stokes problem [26] and the Navier–Stokes problem [27] in three dimensions by a combined BEM and FEM scheme. Extension of the ELBEM model for three-dimensional Navier–Stokes equations in velocity–vorticity form will be presented in one of our future papers.

6. CONCLUDING REMARKS

An accurate Eulerian–Lagrangian BEM for solving the velocity–vorticity Navier–Stokes equations is proposed for the first time by the combination of the ELM and the BEM. The

Poisson-type velocity equations are solved using the general boundary integral technique with domain integration for the source terms and the vorticity boundary conditions are exactly determined. The vorticity transport equation is solved using the ELBEM on a transformed characteristic domain. By the combination of the ELM and the BEM, the BEM is made easier to handle the variable velocity field. Here the results of two-dimensional Navier–Stokes problems with low–medium Reynolds numbers in a typical square cavity flow are presented. A comparison with other numerical models demonstrates the feasibility of the present ELBEM model.

ACKNOWLEDGMENTS

The work reported in this paper was supported by the National Science Council of Taiwan. It is greatly appreciated.

REFERENCES

1. Fasel H. Investigation of the stability of boundary layers by a finite-difference model of the Navier–Stokes equations. *Journal of Fluid Mechanics* 1976; **78**: 355–383.
2. Dennis SCR, Ingham DB, Cook RN. Finite-difference methods for calculating steady incompressible flows in three dimensions. *Journal of Computational Physics* 1979; **33**: 325–339.
3. Gunzburger MD, Peterson JS. On finite element approximations of the streamfunction–vorticity and velocity–vorticity equations. *International Journal for Numerical Methods in Fluids* 1988; **8**: 1229–1240.
4. Skerget L, Rek Z. Boundary-domain integral method using a velocity–vorticity formulation. *Engineering Analysis with Boundary Elements* 1995; **15**: 359–370.
5. Power H, Wrobel LC. *Boundary Integral Methods in Fluid Mechanics*. Computational Mechanics Publications: Southampton, 1995.
6. Brebbia CA, Telles JCF, Wrobel LC. *Boundary Element Techniques—Theory and Applications in Engineering*. Springer: Berlin, 1984.
7. Ikeuchi M. Transient solution of convective diffusion problem by boundary element method. *Transactions of IECE Japan* 1985; **E68**(7): 435–440.
8. Sharif MAR, Busnaina AA. Assessment of finite difference approximations for the advection terms in the simulation of practical flow problems. *Journal of Computational Physics* 1988; **74**: 143–176.
9. Heinrich JC, Huyakorn PS, Zienkiewics OC, Mitchell AR. An upwind finite element scheme for two-dimensional convective transport equation. *International Journal for Numerical Methods in Engineering* 1977; **11**: 131–143.
10. Neuman SP. A Eulerian–Lagrangian numerical scheme for the dispersion–convective equation using conjugate space–time grids. *Journal of Computational Physics* 1981; **41**: 270–294.
11. Neuman SP. Adaptive Eulerian–Lagrangian finite element method for advection–dispersion. *International Journal for Numerical Methods in Engineering* 1984; **20**: 321–337.
12. Li CW. Advective–dispersion simulation by minimization characteristics and alternate direction-explicit methods. *Applied Mathematical Modeling* 1991; **15**: 616–623.
13. Liggett JA. *Fluid Mechanics*. McGraw-Hill: New York, 1994.
14. Fusegi T, Farouk B. Predictions of fluid and heat transfer programs by the vorticity–velocity formulation of the Navier –Stokes equations. *Journal of Computational Physics* 1986; **65**: 227–243.
15. Carslaw HS, Jaegar JC. *Conduction of Heat in Solids* (2nd edn). Clarendon Press: Oxford, 1959.
16. Liu HH, Dane JH. An interpolation-corrected modified method of characteristics to solve advection–dispersion equations. *Journal of Advances in Water Resources* 1996; **19**: 359–368.
17. Burgraff OR. Analytic and numerical studies of structure of steady separated flows. *Journal of Fluid Mechanics* 1966; **24**: 131–151.
18. Ghia U, Ghia KN, Shin CT. High-Re solutions for incompressible flow using the Navier –Stokes equations and a multi-grid method. *Journal of Computational Physics* 1982; **48**: 387–411.
19. Ghia KN, Hamkey Jr WL, Hodge JK. Use of primitive variables in the solution of incompressible Navier–Stokes equations. *AIAA Journal* 1979; **17**: 298–301.

20. Young DL, Lin QH. Application of finite element method to 2D flows. In *Proceedings of the Third National Conference on Hydraulic Engineering*, Young DL (ed.). National Taiwan University: Taipei, 1986; 223–242.
21. Thomadakis M, Leschziner M. A pressure-correction method for the solution of incompressible viscous flows on unstructured grids. *International Journal for Numerical Methods in Fluids* 1996; **22**: 581–601.
22. Giannattasio P, Napolitano M. Optimal vorticity conditions for the node-centered finite-difference discretization of the second-order vorticity–velocity equations. *Journal of Computational Physics* 1996; **127**: 208–217.
23. Liao SJ, Zhu JM. A short-note on high-order streamfunction–vorticity formulations of 2D steady state Navier–Stokes equations. *International Journal for Numerical Methods in Fluids* 1996; **22**: 1–9.
24. Huang H, Seymour BR. The no-slip boundary condition in finite difference approximations. *International Journal of Numerical Methods in Fluids* 1996; **22**: 713–729.
25. Young DL, Her BC, Wang YF. Three-dimensional mathematical modeling of pollutant transport in stratified estuaries. In *Environmental Hydraulics*, Lee JH, Jayawardena AW, Wang ZY (eds). Balkema: Rotterdam, 1999; 93–97.
26. Young DL, Liu YH, Eldho TI. Three-dimensional Stokes flow solution using combined boundary element and finite element methods. *Chinese Journal of Mechanics* 1999; **15**: 169–176.
27. Young DL, Liu YH, Eldho TI. A combined BEM–FEM model for the velocity–vorticity formulation of the Navier–Stokes equations in three-dimensions. *Engineering Analysis with Boundary Elements* 2000; **24**: 307–316.

